Hindawi
Advances in Civil Engineering
Volume 2018, Article ID 6953165, 11 pages
https://doi.org/10.1155/2018/6953165

Research Article

Effects of Particle Size on Fault Gouge Frictional Characteristics and Associated Acoustic Emission

Yang Liu[1], **Cai-Ping Lu**[1,2], **Tong-bin Zhao**[3] and **Heng Zhang**[1]

[1]*Key Laboratory of Deep Coal Resource Mining (Ministry of Education), School of Mines, China University of Mining and Technology, Xuzhou, Jiangsu 221116, China*
[2]*Department of Civil Engineering and Lassonde Institute, University of Toronto, Toronto, ON, Canada M5S 1A4*
[3]*State Key Laboratory of Mining Disaster Prevention and Control Co-founded by Shandong Province and the Ministry of Science and Technology, Shandong University of Science and Technology, Qingdao, Shandong 266590, China*

Correspondence should be addressed to Cai-Ping Lu; cplucumt@126.com

Received 6 January 2018; Accepted 25 February 2018; Published 1 April 2018

Academic Editor: Fengqiang Gong

Our experimental work was designed to explore the particle size effect of simulated fault gouge on slip characteristics by the conventional double-direct shear friction configuration combined with acoustic emission (AE). The following conclusions were drawn: (1) smaller particles allow for an initially higher compaction rate at a higher speed and longer duration for force chain formation and destruction. The larger the particle size is, the higher the slipping displacement rate is; (2) the smaller the particle size is, the larger the friction coefficient is, and thus the higher the fault strength is. In addition, the larger the shear velocity is, the higher the fault strength is; (3) the smaller the particle size is, the higher the shear stress drop generated by the stick-slip is, and the stronger the dynamic slip intensity for a stick-slip period is; and (4) surface defects of forcing blocks possibly help to embed foregoing "stability" and "stable sliding" into the normal stick-slip stage. Especially, the "stable sliding" is possibly related to formation of stubborn force chains. These findings may shed some insights into further clarification of slipping characteristics and discrimination of precursory signs of fault dynamic instability with different-sized gouge particles.

1. Introduction

Faults produce granular wear material continuously due to shearing and friction between two slipping surfaces. As fault gouge, the variation in the mineral composition, particle size, and thickness of the wear material is commonly significant. In general, the two key factors, material and structure of fault gouge, dominate the frictional characteristics of fault zone including fabric development and shear localization with slip. At present, the characteristics of fault gouge have been investigated fruitfully by in situ surveys, laboratory, and numerical simulations to obtain a better understanding of fault mechanics [1–13]. Friction is often characterized as a surface property, but frictional strength of a granular layer and its variations with slip rate and slipping history are also dependent on bulk material properties [14, 15]. For example, the famous San Andreas fault is characterized by anomalously low frictional strengths [16, 17]. However, there is still a lack of consensus, and Scholz [18] has argued that such faults are strong.

As a general characteristic of rock friction, the time-dependent increase in the static friction coefficient under the conditions of changing test conditions and slip surface properties of fault has been repetitively verified [19–24]. However, the actual area of adhesive contact of fault slipping planes should be considered for the actual mechanism by increased asperity penetration and ploughing. In addition, by ploughing an asperity surface through the material on the other slipping surface, the friction force may be generated [15, 25, 26].

Generally, the grain characteristics significantly affect the macroscopic friction of a granular material under shear. Mair et al. [27] have shown that the frictional stability of fault depends on the stress distribution throughout sheared

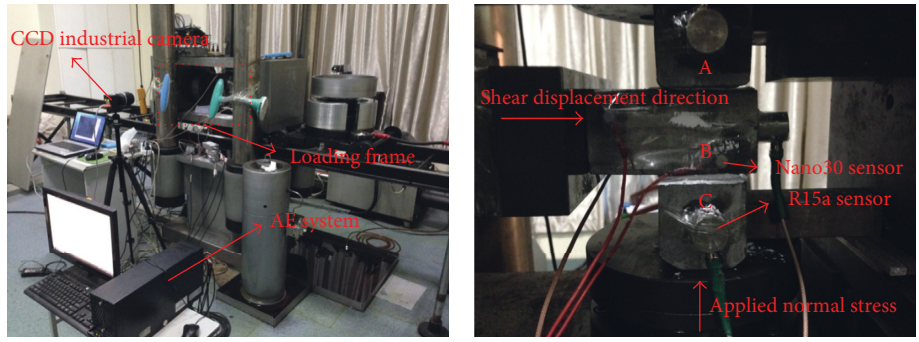

(a) (b)

Figure 1: Testing system and the assemblage of forcing blocks. Note: the upper and lower forcing blocks were each assigned a R15a AE sensor. The center block contained a total of three Nano30 and one R15a AE sensors. (a) Layout of the testing system. (b) Assemblage of the three forcing blocks and AE sensors arrangement.

layers and particle size distribution and angularity. For example, Schleicher et al. [28] discovered that the continuous slip increased fault zones due to reduction of the grain size. Marone et al. [29] believed that the slip rate rose with the thickness and surface roughness of fault gouge. Niemeijer et al. [30, 31] found that the effect of the grains reduced with increase of compaction and revealed that the friction of the talc fabric was higher with the increase of grain size. Collettini et al. [32] found that much of the deformation occurred along zones characterized by particle size reduction and was affected by shear localization. Anthony and Marone [33] interpreted the stick-slip differences associated with gouge layer thickness and particle size based on the mechanics of grain bridges. Knuth and Marone [34] revealed the effects of material properties and surface characteristics of particles on the frictional strength of fault slipping layers.

To date, a number of rate- and state-dependent friction laws have been successfully proposed to physically simulate fault slip that pertains to natural earthquakes. However, the instability essence of fault with different-sized particles of granular layers still remains a matter of much interest characterized by moment release rates much lower than those in other earthquakes [35]. In addition, there are relatively few detailed laboratory studies of acoustic emission (AE) characteristics during the complete slip process of different-sized granular gouge layers, and therefore, we attempted to shed light on the corresponding AE characteristics associated with fault slip by performing conventional double-direct shear tests.

2. Conventional Double-Direct Shear Tests of Simulated Fault

2.1. Experimental System. The experimental system mainly includes a rock testing machine and PCI-2 digital AE monitoring apparatus, as shown in Figure 1(a). The testing machine, with a maximum axial force of 2000 kN, consists of two separate hydraulic loading frames that directly apply normal and shear loads to a sample by electronic servo-controlled feedback systems, and the vertical and horizontal

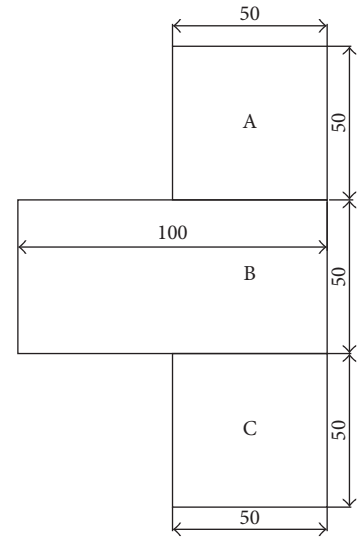

Figure 2: Sample arrangement. Note: the length unit is mm.

strokes are 0–100 mm and 0–50 mm, respectively. The CCD (Basler A641f CCD) industrial camera can monitor the displacement of the samples by collecting the speckle images of the surface of the samples. The AE system uses two different types of sensors, Nano30 and R15a cylindrical sensors, whose dimensions are 8 (diameter) × 8 mm (height) and 19 (diameter) × 22 mm (height), respectively. The frequency response range of the Nano30 sensor is 125–750 kHz and that of the R15a sensor is 50–200 kHz. A total of six channels were employed to collect AE signals.

2.2. Samples. Most fault zones can be modelled by using three mechanical elements: a gouge zone with wall rock on both sides. Rock samples were obtained from borehole cores of a coal mine located at the hanging wall of a thrust fault. The lithology is a coarse sandstone. In lab, the cores were cut to be rectangular parallelepiped with the dimensions of 50 mm (length) × 50 mm (width) × 100 mm (height) and 50 mm (length) × 50 mm (width) × 50 mm (height), respectively; among that, the size of Sample B is 50 mm

Table 1: The parameters of four experimental setups.

Samples number	Normal stresses (MPa)	Particle size (μm)	Shear velocity (μm/s)
Sample 1	2	23	5
Sample 2	2	23	2
Sample 3	2	8.5	2
Sample 4	2	106	5

(length) × 50 mm (width) × 100 mm (height), and the size of Samples A and C is 50 mm (length) × 50 mm (width) × 50 mm (height), and the sample arrangement is shown in Figure 2. Each assemblage included three identical cuboids labeled upper, middle, and lower blocks as A, B, and C, respectively, and two layers of sediment were sandwiched between three forcing blocks. To simulate the roughness of fault, the gouge layers of dry granular quartz powder (the initial particle size is 8.5, 23, and 106 μm, resp.) from a specialized company were sheared. Gouge layers were constructed using a specially designed leveling jig to an initial thickness of 2 mm.

2.3. Methodology. For a conventional double-direct shear friction test, samples consisted of gouge layers sandwiched between forcing blocks in a triple block geometry, as shown in Figure 1(b). Two granular layers were sheared simultaneously between three blocks at constant normal stresses of 2 MPa (Table 1). The vertical ram of the press machine applied a constant normal force and the horizontal ram supported shear traction. Layer dimensions were 5 cm × 5 cm whose thickness is 2 mm. The central block was longer in the shear direction so that up to 5 cm of slip can be achieved. For our sample geometry, slip and friction were accommodated within both gouge layers. The evenly spaced grooves were manufactured on shear surfaces of the forcing blocks, and the coarse sandstone blocks were roughened.

Normal stress was maintained constant in load-feedback servocontrol, and shear stress was then applied by driving the horizontal-oriented ram right and pushing the central block through the shear layers by the type of displacement feedback with fixed shear velocity of 5 or 2 μm/s. Both normal and shear stresses were measured with a precision of 0.1 kN, and displacements of the horizontal and vertical rams were measured by using displacement transducers. When the horizontal ram drives the central block right to produce shear force, the AE system will begin to operate and record signals. Ultimately, when the assemblage generates instability failure or the shear displacement reaches the horizontal stroke of the press machine, the test will be ended. Simultaneously, the AE acquisition is also paused.

Our experiments were designed to explore the transition process from stable slip to stick-slip and the corresponding AE characteristics with covariation of recurrence and shear stress drop during gouge friction of simulated fault with different-sized particles. The parameters of four experimental setups are shown in Table 1.

3. Results and Analysis

Due to similar observations of six AE sensors by critical discrimination, the frequency range of the Nano30 sensor is much larger than that of R15a sensor; therefore, the Nano30 sensor with the relatively large frequency range of 125–750 kHz on the upper forcing block was selected to analyze the AE characteristics during gouge slip and friction.

3.1. Variations of Shear Stress and AE Energy Associated with Gouge Slip at Different Stages

3.1.1. Partition of Different Slip Stages of Gouge Layers. According to Table 1, with the exception of particle size of each couple gouge, consisting of Samples 1 and 4 (23 μm and 106 μm) and Samples 2 and 3 (23 μm and 8.5 μm), the conditions are identical across these two couples. In order to analyze the particle size effect of granular gouge on forcing block slip, the variations of the shear stress and AE energy during the different slip periods of two couples are shown in Figures 3 and 4, and the loading process is divided into several different stages according to the variety characteristic of the stress.

According to Figures 3 and 4, the complete deformation and slip process of simulated fault obviously can be divided into three stages and be defined and concluded in sequence as follows: (1) compaction and equidistribution stage during sliding; (2) stable sliding; and (3) stick-slip instability stage. For particle compaction and equidistribution stage, the experienced loading times of Samples 1 and 4 were 1430 s and 2057 s and that of Samples 2 and 3 were 3560 s and 2930 s, respectively. Therefore, it can be inferred that the smaller the particle size of granular gouge is, the shorter the elapsed time for compaction and equidistribution is.

It was widely believed that particles self-organize to form force chains, which carry the shear traction across a gouge layer, and stress transmission in a granular layer is accomplished through the formation and destruction of force chains, which consist of an anastomosing network of contacting particles that extend between the layer boundaries [20, 36–38]. In Figures 3 and 4, the elapsed times for force chain formation and destruction of Samples 1 and 4 were 530 s and 50 s and that of Samples 2 and 3 were 150 s and 1930 s, respectively. Therefore, it can be clearly verified that force chains exhibit qualitative differences as a function of particle size and shear velocity. For the same shear velocity, the smaller the particle size is, the longer the elapsed time for force chain formation and destruction is.

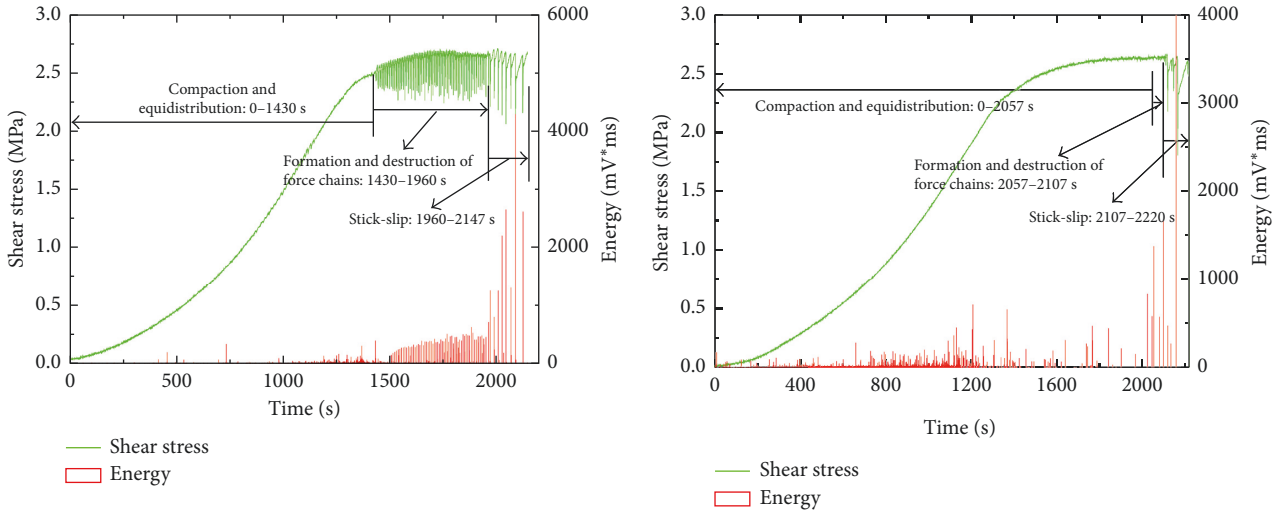

Figure 3: Variations of shear stress and AE energy of (a) Sample 1 and (b) Sample 4.

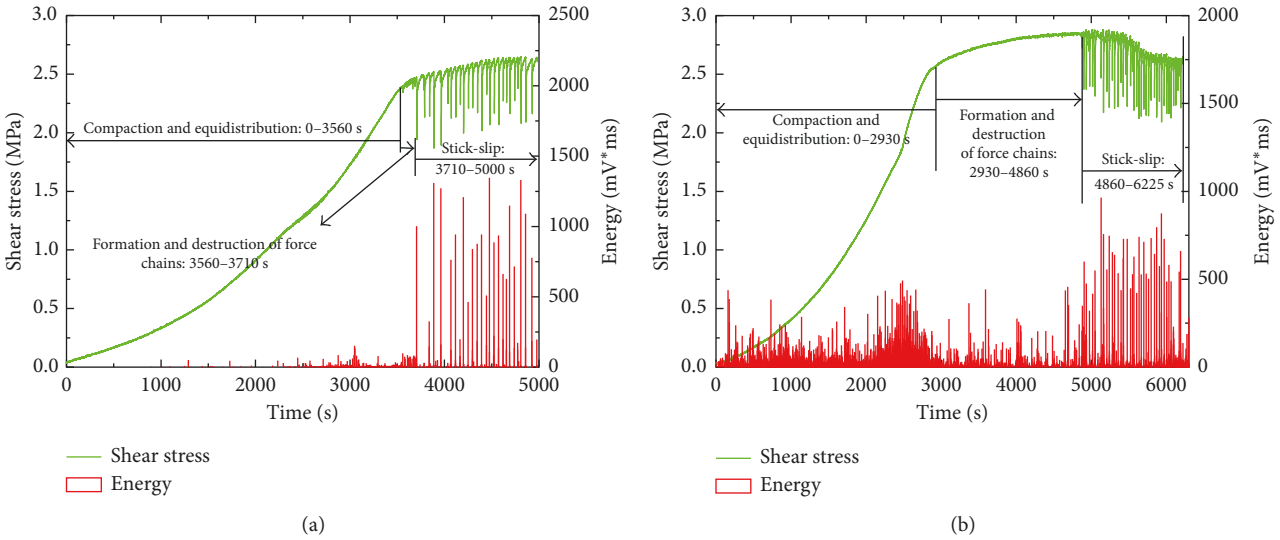

Figure 4: Variations of shear stress and AE energy of (a) Sample 2 and (b) Sample 3.

Unstable sliding is thought to deform by the continuous development and failure of force chains [4, 10, 27, 39, 40]. For unstable sliding regimes, we observed shear stress drop, recurrence interval, preseismic slip, and dynamic slip. In addition, the stable sliding and then episodic sliding as precursory signs of stick-slip were also captured prior to stick-slip according to the relatively lower AE energy distribution.

3.1.2. Correlation between Particles Size, Shear Velocity, and Strength of Simulated Fault. It can be obtained that the maximum shear stress values of Samples 1–4 were 2.706, 2.6496, 2.87976, and 2.65848 MPa, respectively. Based on the comprehensive consideration of particle sizes, shear velocities, and maximum shear stresses of Samples 1–4, it can be extrapolated that the smaller the particle size of granular gouge is, the larger the friction coefficient is (the bigger the actual contact area between both gouge layers is), and therefore the higher the simulated fault strength is. In addition, the larger the shear velocity of gouge layer is, the higher the fault strength is.

3.1.3. Correlation between Particles Size and the AE Energy Generated by Stick-Slip. According to the AE energy distributions of four samples, the energy values of the first and second slipping stages are obviously smaller than that of the third stick-slip stage. To fairly analyze the relationship between the AE energy and particles size across different shear velocities, combined with the consideration of 100 s stick-slip period of Sample 4, the 100 s duration (Sample 1: 1960–2060 s; Sample 4: 2107–2207 s) from stick-slip periods was extracted (Figure 5). Similarly, the duration of 1000 s

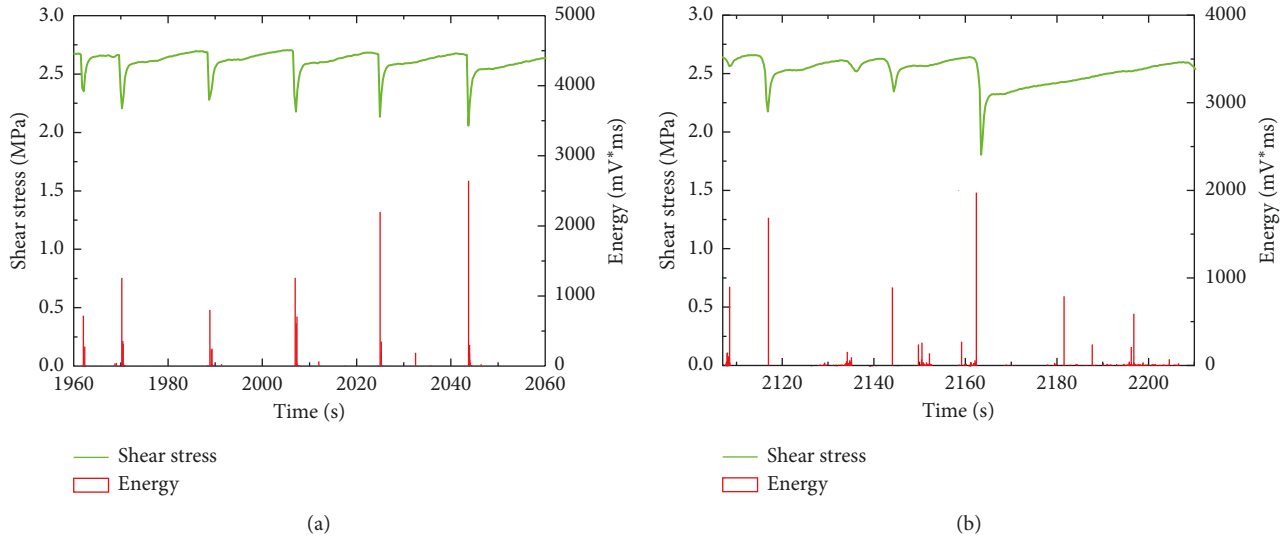

Figure 5: Relationship between shear stress and AE energy of (a) Sample 1 and (b) Sample 4.

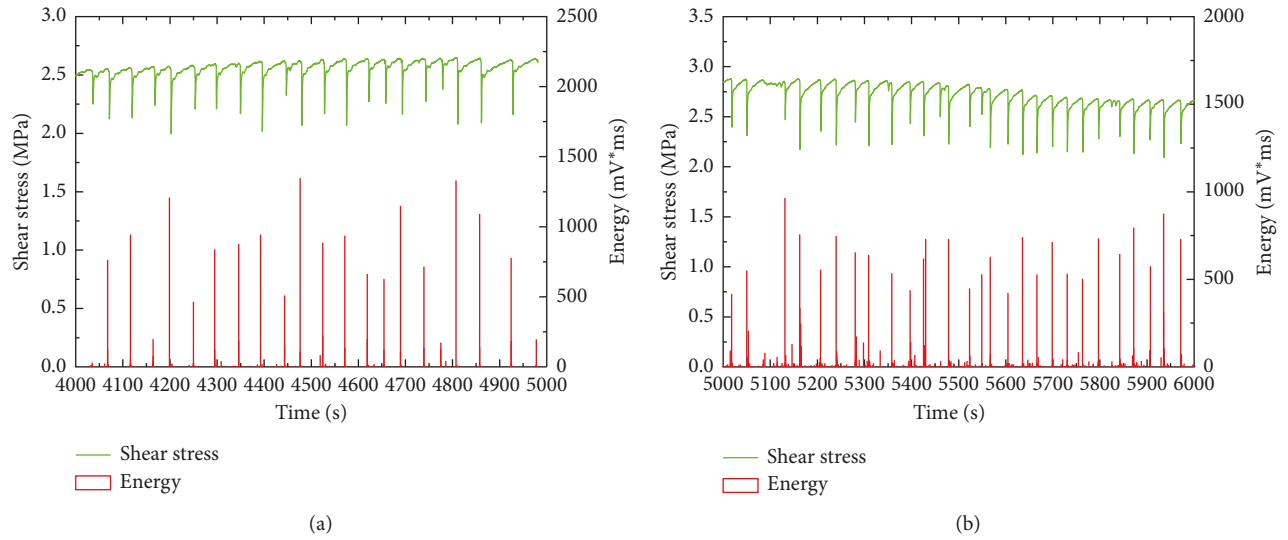

Figure 6: Relationship between shear stress and AE energy of (a) Sample 2 and (b) Sample 3.

(Sample 2: 4000–5000 s; Sample 3: 5000–6000 s) was also extracted Figure 6).

At the stick-slip stage, the simulated fault remains apparently stuck for some period of time, analogous to a natural earthquake recurrence interval, and then fails, slipping rapidly and producing a shear stress drop through unloading of elastic strain stored in the rock and testing machine. AE peaks periodically appear with the recurrent stick-slip events, and the number of AE peaks is strictly equivalent to stick-slip events with the exception of Sample 4 (the reason was explained in Section 4.2).

Due to shorter stick-slip durations of Samples 1 and 4, the influencing effect of particle size on the released energy and shear stress drop during stick-slip cannot be comprehensively analyzed. Therefore, AE energies and shear stress drops of stick-slip events selected from Samples 2 and 3 with significant stick-slip process were, sequentially and respectively, calculated and listed, and then the variations of AE energy and shear stress drop with particle size were further analyzed, as shown in Figure 7 (the horizontal time coordinate of each stick-slip event should be equal to its actual occurrence time minus the statistically starting time).

From Figure 7, the AE total energy value of Sample 3 is larger than that of Sample 2 for the same duration. Therefore, it can be inferred that the smaller the particle size of granular gouge is, the higher the released total energy generated by the stick-slip is, and the larger the stick-slip event count is. However, the AE average energy of Sample 3 is slightly smaller than that of Sample 2, which indicates that the average stick-slip dynamic intensity will enhance with the increasing particle size. In addition, the total and average shear stress drops of Sample 3 are larger than that of Sample 2 for the same duration. Combined with the variation of AE total energy, it can be inferred that the smaller the particle

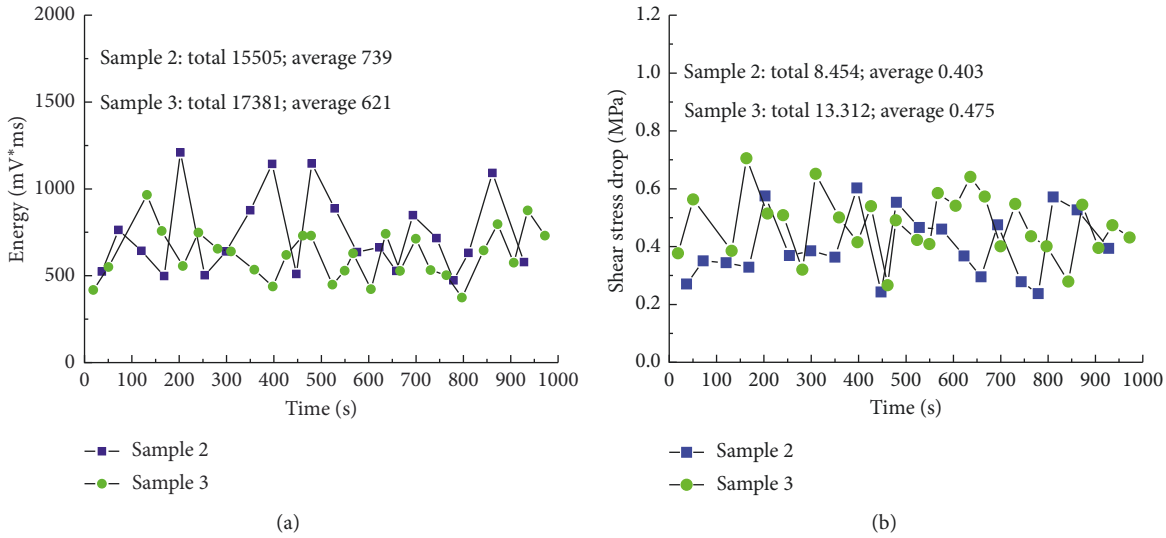

Figure 7: Comparison of AE energy and shear stress drop during the statistical stick-slip periods of Samples 2 and 3. (a) AE energy. (b) Shear stress drop.

size of the granular gouge is, the higher the shear stress drop generated by the stick-slip is, and therefore the stronger the unstably dynamic slip intensity for a stick-slip period is.

In summary, the systematic differences due to particle size and shear velocity of gouge layers were observed, and the following three points can be concluded:

(a) Slip process of simulated fault is divided into three stages based on variation of shear stress: compaction and equidistribution stage of gouge particles; stable slipping; and stick-slip instability stage, respectively. At the compaction stage, shear stress steadily rises along with the gradual increase of increment rate and ultimately begins to transform into slight fluctuation. With ongoing compaction, the smallest particles will stop compacting, either because they are completely dissolved or because the contact area is too large, effectively decreasing the macroscopic compaction rate. At the second stage as precursor of stick-slip, shear stress begins to recurrently undulate with smaller amplitude, which still belongs to stable slipping. Stable sliding initiates at a point and then spreads out with an accelerating sliding velocity until the stick-slip instability. At stick-slip stage, shear stress is obviously larger than the critical value of kinetic friction coefficient of gouge layer, simultaneously accompanied with stress drop, recurrence interval, preseismic slip, and dynamic slip.

(b) The smaller the particle size of the granular gouge is, the larger the friction coefficient is, and the higher the fault strength is. In addition, the smaller the particle size is, the shorter the compaction time is, and the higher the total released energy generated by the stick-slip is.

(c) Compared with the compaction stage, the intensity of fault prior to stick-slip is relatively higher, and shear stress reaches the maximum static friction resistance. The second stage as stable sliding can be defined as the precursory period of stick-slip. The smaller the particle size of the sheared gouge is, the faster the shear velocity is (for the same particle size) and thus the more significant the precursory effect of the stick-slip is. Simultaneously, the higher the shear stress drop generated by the stick-slip is, and the stronger the dynamic slip intensity for a stick-slip period is.

3.2. Variations of Displacement State Associated with Gouge Slip at Different Stages. In order to further analyze the variations of displacement state of four samples during the complete slipping process, the correlation between shear stress, AE energy and event count, and displacement was clearly revealed, as shown in Figures 8 and 9, and the loading process was divided into several different stages according to the variety characteristics of the stress and displacement.

In order to further reveal the relationship between particle size and displacement, 100 s duration (Sample 1: 1960–2060 s; Sample 4: 2107–2207 s) from stick-slip periods was extracted. Similarly, 1000 s duration (Sample 2: 4000–5000 s; Sample 3: 5000–6000 s) was also extracted. The variation of stick-slip displacement of Samples 1–4 is shown in Figure 10 (the horizontal time coordinate of each stick-slip event should be equal to its actual occurrence time minus the statistically starting time).

According to Figures 8–10, the following three key points can be addressed:

(a) The complete slipping process of fault gouge can be considered as four stages. For the stability stage, both shear stress and displacement slowly rise. AE does not obviously appear, and the energy and event count are almost equal to zero except for Sample 3. At the stable sliding stage, both shear stress and displacement quickly increase due to accomplishment of compaction, and AE also starts to significantly manifest, especially for the fast sliding stage of Sample 4. Totally, shear stress steadily increases prior to the stick-slip stage with the exception of Sample 1, simultaneously accompanied

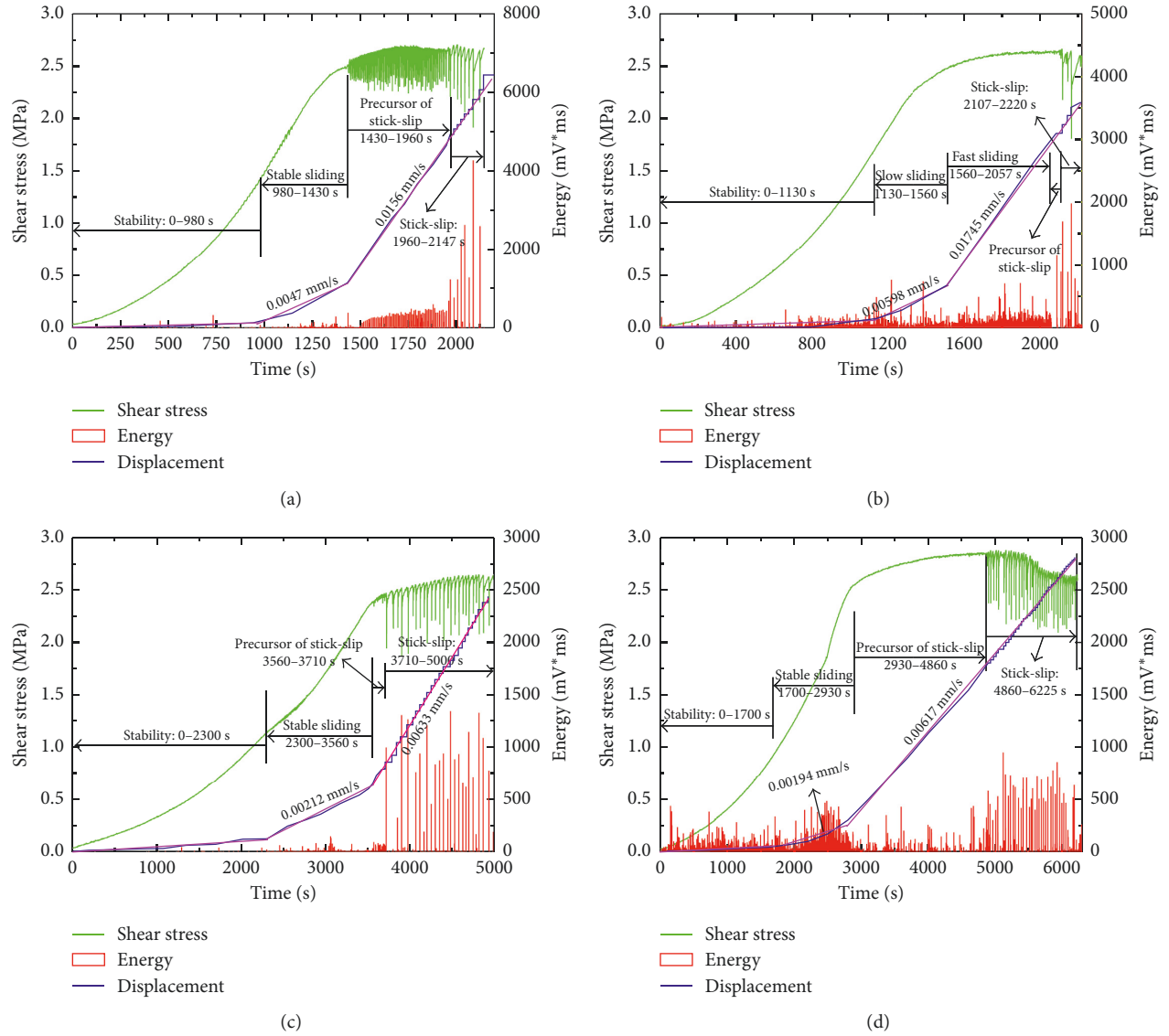

FIGURE 8: Correlation between shear stress, AE energy, and displacement during slipping. Note: for Sample 1, the displacement value (unit: mm) is 6 times of its shear stress value. Similarly, the multiples of Samples 2–4 displacement are 5, 9, and 7, respectively. (a) Sample 1. (b) Sample 4. (c) Sample 2. (d) Sample 3.

with small-amplitude undulation. Additionally, the incremental rate of displacement also obviously rises, and AE intensity enhances to some extent with fluctuation of shear stress. However, the total level of AE intensity dominantly depends on shear stress drop. For stick-slip, all of the slip occurs acoustically, and AE energy reaches the peak with high stress drop, which may be generated by the effect of shear strain localization. In addition, AE peaks periodically appear with the recurrent stick-slip events, and the number of AE peaks is equivalent to stick-slip events. Interestingly, the incremental rate of displacement does not obviously changes compared with the precursor of stick-slip.

(b) According to the approximate regression of displacement curves, it is known that the incremental rates of displacement of Samples 1–4 at the stable sliding stage are 0.0047, 0.00212, 0.00194, and 0.00598 mm/s and that prior to stick-slip and at the stick-slip stage are 0.0156, 0.00633, 0.00617, and 0.01745 mm/s, respectively. By calculation, the displacement velocity prior to and at the stick-slip stage is about 3–3.5 times of that of stable sliding. In addition, on basis of particle size of gouge layer, it can be extrapolated that the larger the particle size is, the faster the shear velocity for Samples 1 and 2 with the same particle size is, and the higher the slipping displacement velocity of the fault gouge is. For each stick-slip event, based on the displacement comparisons of Samples 1 and 4 and Samples 2 and 3, during the statistical stick-slip period (as seen from Figure 10), it can be indicated that particle size is almost positively associated with the slipping displacement.

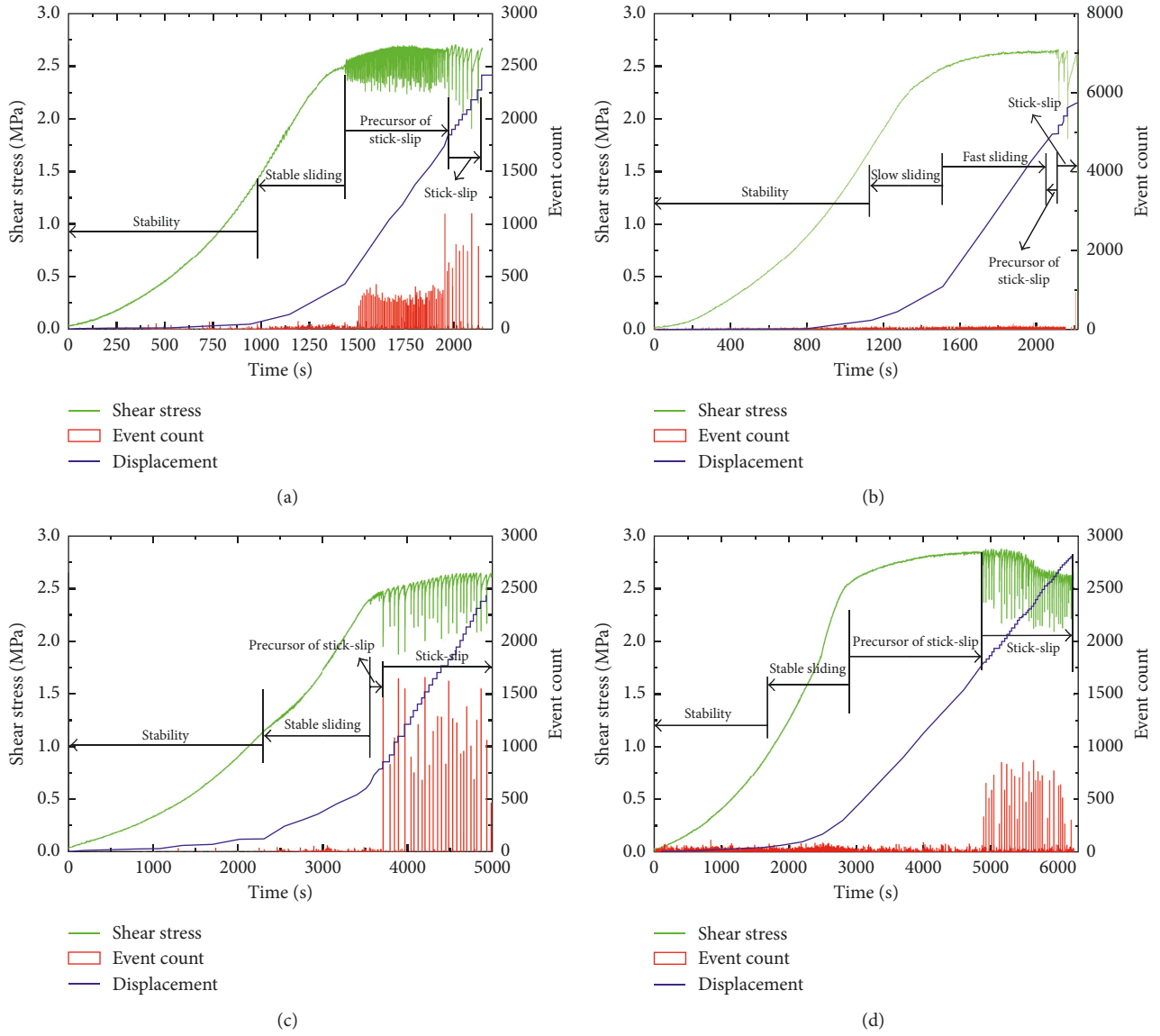

Figure 9: Correlation between shear stress, AE event count, and displacement during slipping. Note: the multiples between displacement (unit: mm) and shear stress value of Samples 1–4 are 6, 5, 9, and 7, respectively. (a) Sample 1. (b) Sample 4. (c) Sample 2. (d) Sample 3.

(c) At the stable sliding stage, shear stress obviously rises, and the slow slips with smaller displacement occur within both gouge layers. Simultaneously, AE appears with lower energy and higher event count. Compared with the stability stage, the overall AE intensity enhances. Prior to stick-slip, the density of AE significantly decreases with small energy release, which indicates the initiation of shear strain localization of contact surfaces and formation of a series of shear failure.

4. Discussions

4.1. Dispersion Analysis of Experimental Results on Granular Size Effects. Experimental results on shear of different-sized particles presented in Figure 7 are compared only qualitatively based on the average and total AE energy and shear stress drop. Due to the dispersion of results to some extent, we further analyzed and then proved that the results belong to the same general variation based on one-way analysis of variance (ANOVA). For example, for Samples 2 and 3, taking the influencing factor of particle size into account, the p values of AE energy and shear stress drop are 0.0375 and 0.0277, respectively, less than 0.05, which indicates that the influencing level of particle size of the granular gouge layer on stick-slip instability intensity is significant.

Similarly, for Samples 2 and 3 (Figure 10(b)), the p value of slipping displacement is 0.0129, less than 0.05. Therefore, the particle size can significantly influence slipping displacement of simulated fault during stick-slip. However, for Samples 1 and 4 (Figure 10(a)), the p value of slipping displacement is 0.1087, obviously larger than 0.05, and therefore the nonsignificant difference may be related to the shorter statistical stick-slip period.

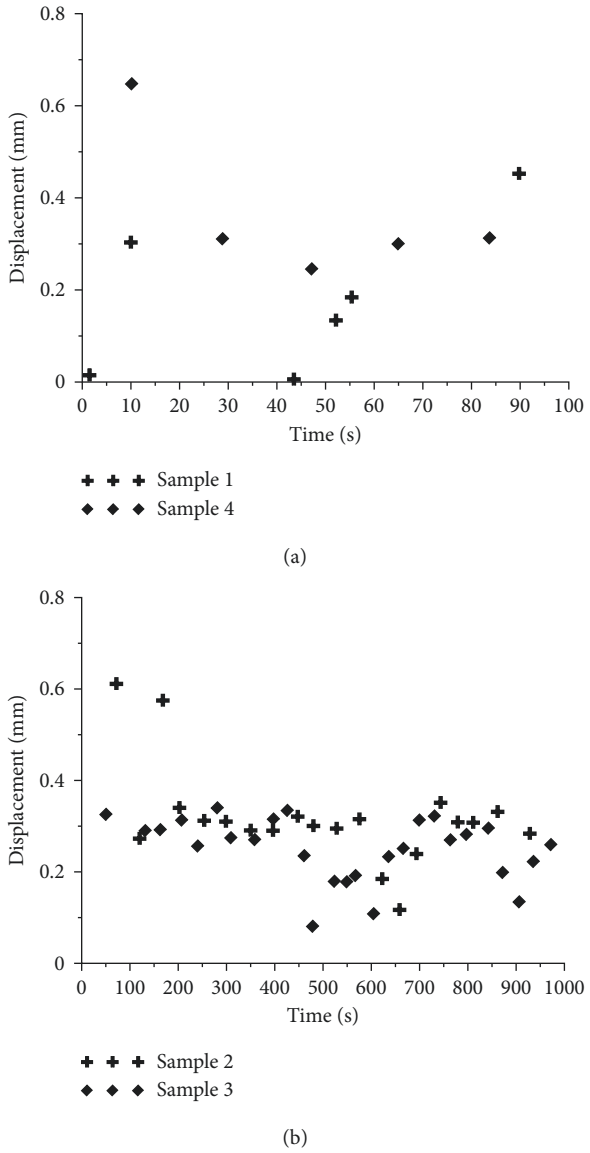

Figure 10: Displacement variations of Samples 1–4 during the statistical stick-slip periods. (a) Samples 1 and 4. (b) Samples 2 and 3.

4.2. Occurrence of Stability and Stable Sliding Embedded in Stick-Slip Stage. There are AE events even when no major slip event is observed as well as several minor slip events for Sample 4, and the two periods are marked in Figure 11(a). The first period from 2149.7 to 2152 s belongs to the stability stage without obvious displacement variation, and the second period from 2181 to 2196.8 s approximately manifests uniform sliding, as shown in Figure 11(c). Interestingly, the foregoing stability and stable sliding embedded in the stick-slip stage disturb the regular sequence of simulated fault gouge slip. Maybe, the interference of "stability" is generated by particle compaction and equidistribution again due to surface defects such as significant roughness of forcing blocks where the slip position reaches. When particle compaction and equidistribution occurs, the small energy AE events will generate. In addition, the occurrence of "stable sliding" with uniform slipping speed is possibly related to the formation of

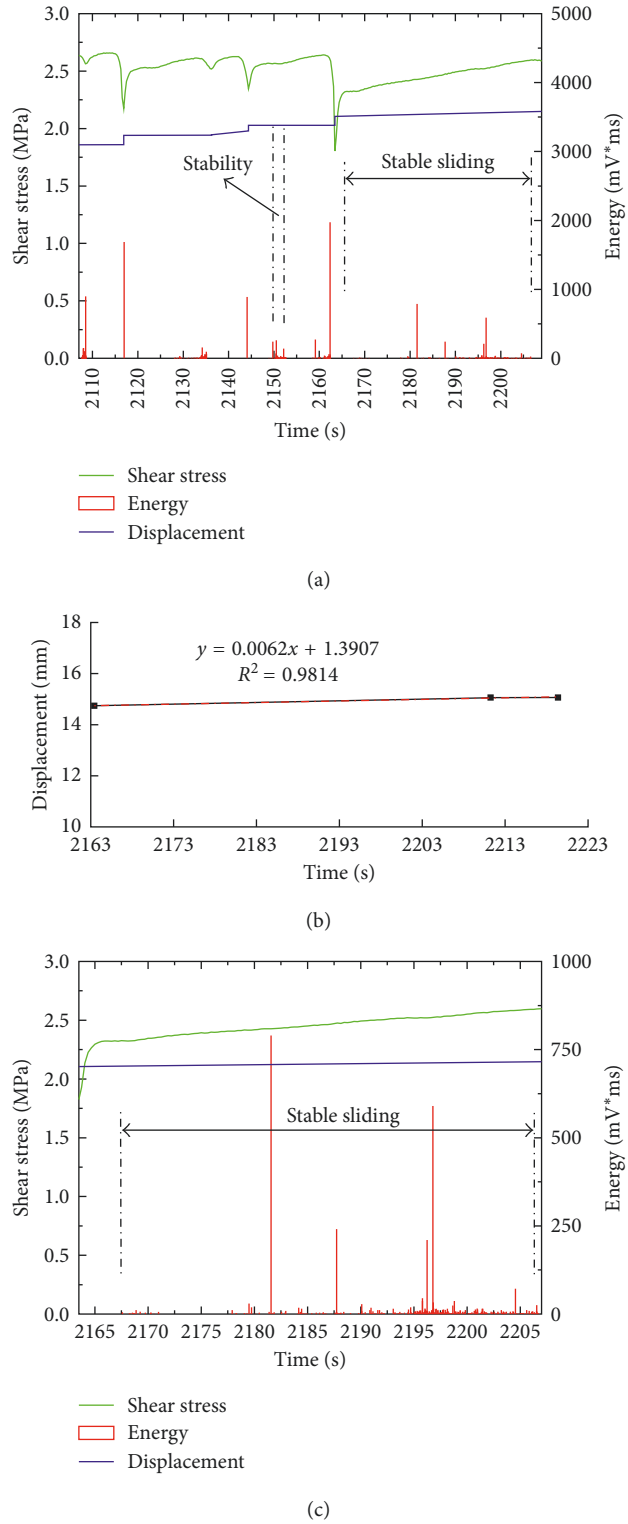

Figure 11: Correlation between shear stress, AE energy, and slipping displacement during stick-slip of Sample 4. (a) Shear stress, AE energy, and slipping displacement. (b) Slipping displacement curve and its linear regression. (c) Enlargement of the stable sliding stage in (a).

stubborn force chains maintaining fairly considerable duration, and the relatively high-energy AE events will appear with the stable sliding, as shown in Figure 11(b).

5. Conclusions

Compacted aggregates of dry quartz particles, with 8.5, 23, and 106 μm in size, were deformed to simulate the mechanical behavior of quartz fault gouge and help to explain the effect of particle size and corresponding AE characteristics associated with fault slip. The following conclusions were addressed:

(1) Particle size effect on slipping stages: smaller particles allow for an initially higher compaction rate at a higher speed and longer duration for force chain formation and destruction combined with faster shear velocity. In addition, the larger the particle size is, the faster the shear velocity for same particle size is, and the higher the slipping displacement rate is.

(2) Particle size effect on dynamic slip intensity: the smaller the particle size is, the higher the shear stress drop generated by the stick-slip is, and the stronger the dynamic slip intensity for a stick-slip period is. Therefore, the particle size can significantly influence stick-slip instability intensity and slipping displacement of simulated fault.

(3) Particle size effect on AE characteristics generated by slip: at the stable sliding stage, AE appears with lower energy and higher event count. Prior to stick-slip, the density of AE significantly decreases with small energy release. At the stick-slip stage, AE peaks periodically appear with the recurrent stick-slip events, and the number of AE peaks is equivalent to stick-slip events. Interestingly, the incremental rate of displacement does not obviously changes compared with the precursor of stick-slip.

(4) Surface defects of forcing blocks accommodating gouge particles possibly help to embed foregoing "stability" and "stable sliding" into the normal stick-slip stage. Especially, the "stable sliding" is possibly related to the formation of stubborn force chains maintaining fairly considerable duration, and the relatively high-energy AE events appear with the stable sliding.

Conflicts of Interest

The authors declare that there are no conflicts of interests regarding the publication of this paper.

Acknowledgments

The authors wish to express their thanks to the collaborative funding support from the National Natural Science Foundation of China (51574225), the Fundamental Research Funds for the Central Universities (2015XKZD04), a project funded by the Priority Academic Program Development of Jiangsu Higher Education Institutions (PAPD), and the Postgraduate Research & Practice Innovation Program of Jiangsu Province (KYCX17_1554).

References

[1] J. T. Engelder, "Cataclasis and the generation of fault gouge," *Geological Society of America Bulletin*, vol. 85, no. 10, pp. 1515–1522, 1974.

[2] F. M. Chester and J. M. Logan, "Implications for mechanical properties of brittle faults from observations of the Punchbowl Fault Zone, California," *Pure and Applied Geophysics PAGEOPH*, vol. 124, no. 1-2, pp. 79–106, 1986.

[3] Z. Reches, "Evolution of fault patterns in clay experiments," *Tectonophysics*, vol. 145, no. 1-2, pp. 141–156, 1988.

[4] R. L. Biegel, C. G. Sammis, and J. H. Dieterich, "The frictional properties of a simulated gouge having a fractal particle size distribution," *Journal of Structural Geology*, vol. 11, no. 7, pp. 827–846, 1989.

[5] S. H. Haines, B. Kaproth, C Marone et al., "Shear zones in clay-rich fault gouge: a laboratory study of fabric development and evolution," *Journal of Structural Geology*, vol. 51, pp. 206–225, 2013.

[6] D. R. Scott, C. Marone, and C. G. Sammis, "The apparent friction of granular fault gouge in sheared layers," *Journal of Geophysical Research*, vol. 99, no. B4, pp. 7231–7246, 1994.

[7] M. R. Prante and J. P. Evans, "Pseudotachylyte and fluid alteration at seismogenic depths (Glacier Lakes and Granite Pass Faults, Central Sierra Nevada, USA)," *Pure and Applied Geophysics*, vol. 172, no. 5, pp. 1203–1227, 2015.

[8] F. M. Chester and J. S. Chester, "Ultracataclasite structure and friction processes of the Punchbowl fault, San Andreas system, California," *Tectonophysics*, vol. 295, no. 1-2, pp. 199–221, 1998.

[9] P. Mora and D. Place, "Numerical simulation of earthquake faults with gouge: toward a comprehensive explanation for the heat flow paradox," *Journal of Geophysical Research: Solid Earth*, vol. 103, no. B9, pp. 21067–21089, 1998.

[10] K. Mair and S. Abe, "3D numerical simulations of fault gouge evolution during shear: grain size reduction and strain localization," *Earth and Planetary Science Letters*, vol. 274, no. 1-2, pp. 72–81, 2008.

[11] J. K. Morgan, "Numerical simulations of granular shear zones using the distinct element method: 2. Effects of particle size distribution and interparticle friction on mechanical behavior," *Journal of Geophysical Research: Solid Earth*, vol. 104, no. B2, pp. 2721–2732, 1999.

[12] E. Aharonov and D. Sparks, "Rigidity phase transition in granular packings," *Physical Review E*, vol. 60, no. 6, pp. 6890–6896, 1999.

[13] O. Katz, Z. Reches, and G. Baer, "Faults and their associated host rock deformation: structure of small faults in a quartz-syenite body, southern Israel," *Journal of Structural Geology*, vol. 25, no. 10, pp. 1675–1689, 2003.

[14] E. Rabinowicz, "Stick and slip," *Scientific American*, vol. 194, no. 5, pp. 109–118, 1956.

[15] F. P. Bowden and D. Tabor, *The Friction and Lubrication of Solids: Part II*, Oxford University Press, Oxford, UK, 1964.

[16] A. H. Lachenbruch and J. H. Sass, "Heat flow and energetics of the San Andreas fault zone," *Journal of Geophysical Research: Solid Earth*, vol. 85, no. B11, pp. 6185–6223, 1980.

[17] M. D. Zoback, "Strength of the San Andreas," *Nature*, vol. 405, no. 6782, pp. 31-32, 2000.

[18] C. H. Scholz, "Evidence for a strong San Andreas fault," *Geology*, vol. 28, no. 2, pp. 163–166, 2000.

[19] J. H. Dieterich, "Time-dependent friction in rocks," *Journal of Geophysical Research*, vol. 77, no. 20, pp. 3690–3697, 1972.
[20] C. H. Scholz, P. Molnar, and T. Johnson, "Detailed studies of frictional sliding in granite and implications for earthquake mechanism," *Journal of Geophysical Research*, vol. 77, no. 32, pp. 6392–6406, 1972.
[21] J. T. Engelder, J. M. Logan, and J. Haudin, "The sliding characteristics of sandstone on quartz fault-gouge," *Pure and Applied Geophysics PAGEOPH*, vol. 113, no. 1, pp. 69–86, 1975.
[22] C. H. Scholz and J. T. Engelder, "The role of asperity indentation and ploughing in rock friction : I. Asperity creep and stick-slip," *International Journal of Rock Mechanics and Mining Sciences & Geomechanics Abstracts*, vol. 13, no. 8, pp. 149–154, 1976.
[23] J. T. Engelder and C. H. Scholz, "The role of asperity indentation and ploughing in rock friction: H. Influence of relative hardness and normal load," *International Journal of Rock Mechanics and Mining Sciences & Geomechanics Abstracts*, vol. 13, no. 8, pp. 155–163, 1976.
[24] L. W. Teufel, *The Measurement of Contact Areas and Temperature during Frictional Sliding of Tennessee Sandstone*, M.Sc. thesis, p. 65, Texas A&M University, College Station, TX, USA,1976.
[25] E. Rabinowicz, *Friction and Wear of Materials*, John Wiley, New York, NY, USA, 1965.
[26] J. C. Jaeger and N. G. W. Cook, *Fundamentals of Rock Mechanics*, Methuen Co. Ltd., London, UK, 1969.
[27] K. Mair, K. M. Frye, and C. Marone, "Influence of grain characteristics on the friction of granular shear zones," *Journal of Geophysical Research: Solid Earth*, vol. 107, no. B10, p. 2219, 2002.
[28] A. M. Schleicher, B. A. van der Pluijm, J. G. Solum, and L. N. Warr, "Origin and significance of clay-coated fractures in mudrock fragments of the SAFOD borehole (Parkfield, California)," *Geophysical Research Letters*, vol. 33, no. 16, p. L36313, 2006.
[29] C. Marone, B. Raleigh, and C. H. Scholz, "Frictional behavior and constitutive modeling of simulated fault gouge," *Journal of Geophysical Research*, vol. 95, no. B5, pp. 7007–7025, 1990.
[30] A. Niemeijer, D. Elsworth, and C. Marone, "Significant effect of grain size distribution on compaction rates in granular aggregates," *Earth and Planetary Science Letters*, vol. 284, no. 3-4, pp. 386–391, 2009.
[31] A. Niemeijer, C. Marone, and D. Elsworth, "Fabric induced weakness of tectonic faults," *Geophysical Research Letters*, vol. 37, no. 3, p. L03304, 2010.
[32] C. Collettini, A. Niemeijer, C. Viti et al., "Fault zone fabric and fault weakness," *Nature*, vol. 462, no. 7275, pp. 907–910, 2009.
[33] J. L. Anthony and C. Marone, "Influence of particle characteristics on granular friction," *Journal of Geophysical Research*, vol. 110, no. B8, p. B08409, 2005.
[34] M. Knuth and C. Marone, "Friction of sheared granular layers: role of particle dimensionality, surface roughness, and material properties," *Geochemistry, Geophysics, Geosystems*, vol. 8, no. 3, p. Q03012, 2006.
[35] P. F. Ihmle and T. H. Jordan, "Teleseismic search for slow precursors to large earthquakes," *Science*, vol. 266, no. 5190, pp. 1547–1550, 1994.
[36] S. Tembe, D. A. Lockner, and T. Wong, "Effect of clay content and mineralogy on frictional sliding behavior of simulated gouges: binary and ternary mixtures of quartz, illite, and montmorillonite," *Journal of Geophysical Research*, vol. 115, no. B3, 2010.
[37] L. Molnar, T. M. Toth, and F. Schubert, "Statistical characterization of brittle and semi-brittle fault rocks: a clast geometry approach," *Acta Geodaetica et Geophysica*, vol. 49, no. 4, pp. 527–550, 2014.
[38] M. Ohnaka, Y. Kuwahana, K. Yamamoto et al., "Earthquakes source mechanics," in *Geophysical Monograph Series*, S. Das, J. Boatwright, and C. Scholz, Eds., pp. 13–24, American Geophysical Union, Washington, DC, USA, 1986.
[39] C. G. Sammis and S. J. Steacy, "The micromechanics of friction in a granular layer," *Pure and Applied Geophysics PAGEOPH*, vol. 142, no. 3-4, pp. 777–794, 1994.
[40] M. E. Cates, J. P. Whitmer, J. P. Bouchaud et al., "Jamming, force chains, and fragile matter," *Physical Review Letters*, vol. 81, no. 9, pp. 1841–1844, 1998.